Monte Carlo Scheme for Generation and Relaxation of Dense and Nearly Jammed Random Structures of Freely Jointed Hard-Sphere Chains

Nikos Ch. Karayiannis* and Manuel Laso

Institute for Optoelectronics and Microsystems (ISOM) and ETSII, UPM José Gutiérrez Abascal, 2 E-28006 Madrid, Spain

Received October 10, 2007; Revised Manuscript Received November 30, 2007

ABSTRACT: We describe a general Monte Carlo (MC) suite for the efficient relaxation of dense systems of freely jointed chains of hard spheres for packing densities (φ) ranging from dilute ones ($\varphi \approx 0.1$) up to the vicinity of the maximally random jammed (MRJ) state ($\varphi \approx 0.639$). Key components of the new MC scheme are as follows: (i) modified versions of state-of-the-art chain-connectivity altering moves tailored to function efficiently even for very dense random chain assemblies and (ii) localized MC moves, all executed in an adaptive configurational-bias pattern. Two different athermal systems were simulated consisting of 100 and 50 chains with average lengths $N_{av} = 12$ and 24, respectively, over a wide range of packing densities. In all cases studied, computational efficiency is compared against corresponding results obtained from extensive applications of conventional MC techniques; it is shown that the proposed MC scheme outperforms by several orders of magnitude all existing methods in relaxing the short- and long-range characteristics of the simulated systems and is thus the only available vehicle to generate and equilibrate (and successively characterize) representative model chain configurations near the MRJ state. Structural results, obtained from averaging over very long MC trajectories, show the dependence of bonded geometry (quantified by the bending and torsion angle distributions), chain dimensions (quantified by the end-to-end distance and radius of gyration) and local packing on volume fraction.

I. Introduction

Random packing of dilute, semidilute, and dense systems consisting of either monatomic hard spheres or freely jointed chains of tangent hard spheres has been the focus of extended scientific research over the last decades. While hard spheres constitute the coarsest form of structural representation, they can be used as predictive models for the investigation of a wide range of phenomena and processes.[1−4] One of the most fundamental questions, which a wealth of experimental, theoretical and simulation studies on monatomic liquids tried to address, can be roughly stated as "which is the maximum packing density (φ) that can be achieved for ordered and random structures consisting of identical hard spheres?".

As recently proven by Hales,[5,6] according to the Kepler conjecture (theorem) "in a 3-d Euclidean space no packing of congruent balls has density greater than that of the face-centered cubic packing". The (densest) packing densities of either face-centered cubic (fcc) or hexagonal close packing (hcp) lattices can be readily calculated analytically as $\varphi_{fcc} = \varphi_{hcp} = \pi/\sqrt{18} \approx 0.74048$.[7]

For irregular assemblies of identical hard spheres, early seminal studies provided important findings about structural topology and how these random packings can be treated as geometrical models of relatively simple polyhedral subunits.[8−13] The freezing and melting volume fractions of monatomic hard spheres have been calculated at $\varphi_F \approx 0.494$ and $\varphi_M \approx 0.545$, respectively.[14] The upper limit of density for randomly packed arrays of hard spheres (a state originally referred to as "random close packing" (RCP)) has been estimated by independent methods at $\varphi_{rcp} \approx 0.6366$[15,16] and $0.642 - 0.645$ (through extrapolation).[17] Various algorithms exist for the creation of dense random hard-sphere packings,[18−20] reaching volume fractions up to 0.642−0.645.[3,21] Recently, Torquato and collaborators challenged the mathematically ill-defined RCP term and introduced the concept of "maximally random jammed" (MRJ) state.[22−24] All data reported in their simulations were obtained by event-driven molecular dynamics (MD) simulations[25,26] based on the modified Lubachevsky−Stillinger algorithm.[27]

While there have been a great number of computational studies focusing on random dense packings of monatomic hard spheres, corresponding simulation efforts on irregular assemblies of chain molecules of tangent hard spheres ("pearl-necklace" chains) are relatively quite limited and almost exclusively applied on systems characterized by packing densities quite far from the MRJ state.[28−46] In all simulations of dense systems of irregular assemblies of hard spheres one faces two major challenges: (i) the creation of the initial (random) configuration corresponding to the desired packing density and (ii) the generation of a large number of uncorrelated configurations given that, ideally, all information about packing should be obtained as an average over an extended set of different structures. For monatomic systems the first issue (construction of simulation cell) can be addressed by algorithms like the ones proposed by Jodrey and Tory[18,19] and by Tobochnik and Chapin,[47] while in a second stage collision-driven MD algorithms[48] undertake the task of relaxing the local intersphere packing. For systems of "pearl-necklace" chains, any stochastic or dynamic simulations should respect the holonomic constrains imposed by the bonded geometry of the molecules (where the bond lengths are fixed and equal to the collision diameter). Besides the fact that a construction of an efficient event-driven MD simulation is not quite straightforward for dense systems of chains of tangent hard spheres, it is well-established that MD algorithms provide poor long-range equilibration for dense

* Corresponding author. E-mail: nkarayiannis@etsii.upm.es.

10.1021/ma702264u CCC: $40.75
Published on Web 01/25/2008

systems of long (in particular entangled) chains even through simulations that reach microseconds.[49]

Stochastic Monte Carlo (MC) simulation can be an excellent alternative for the generation and rapid relaxation of dense packings of hard-sphere chains through the design of sophisticated "unphysical" moves which propagate the system through global configurational transitions that otherwise could not be tracked by conventional means (MD). In the last years there has been a scientific blossom in fabricating "clever" MC sampling techniques for either lattice-based or continuum-space simulations. Especially for atomistic, chemically simple (polyethylene-like) macromolecular substances, full-scale equilibration can be achieved within modest time and computational resources through advanced, chain-connectivity altering algorithms (like the "end-bridging" (EB),[50] "double-bridging" (DB),[51] and similar complex schemes[52−54]) accompanied by a set of efficient local counterparts like for example the reptation,[55,56] the continuum configurational bias (CCB)[57,58] and the concerted rotation (ConRot)[59] moves. Albeit being very efficient for sampling atomistic configurations in dilute or semidilute systems, a MC suite (and similar schemes) based on these combinations is not directly applicable to dense structures of "pearl-necklace" chains, since almost all conformational transitions attempted in the course of a typical MC simulation are rejected due to hard-sphere overlaps. Consequently, the fundamental question regarding the MRJ state of hard-sphere chains and how this densest limit compares with the monatomic analog remained an open issue.

Very recently, we introduced a new MC scheme capable of generating and relaxing dense random packings of freely jointed chains of hard spheres even close to the maximally random jammed (MRJ) state.[60] Simulation findings provided information about the bonded geometry (distribution of bending and torsion angles), the chain dimensions (radius of gyration and end-to-end distance) and the radial distribution functions as well as their dependence on packing density.[60] The proposed MC suite is composed of algorithms inspired by successful analog(s) used in atomistic simulations and combines both chain-connectivity altering and localized moves, all specially modified to function even on densely packed simulation cells.

In this paper we give a detailed description of the algorithm behind the MC method (used extensively in ref 60 for dense and nearly jammed random chain packings) and we document its efficiency, in equilibrating the long- and short- range characteristics of the athermal systems, by comparing its performance against available MC schemes. The paper is organized as follows: section II lists the modeled chain systems and the statistical ensembles that were employed in all MC simulations. Section III summarizes the moves that constitute the new MC scheme constructed in the course of the present work. Section IV focuses exclusively on the presentation and description of the new chain-connectivity altering MC moves incorporated here. In section V, we present all results regarding computational efficiency of new MC scheme and about the effect of packing density on bonded geometry, packing and chain dimensions. Finally, the paper is concluded by providing a summary of the main conclusions and by presenting potential applications and extensions of the new MC algorithm.

II. Systems Studied: Statistical Ensemble

All molecules are modeled as freely jointed chains consisting of spheres interacting in pairs through a typical hard-core potential $u(r)$:

$$u(r_{ij}) = \infty, \quad r_{ij} < \sigma$$
$$u(r_{ij}) = 0, \quad r_{ij} \geq \sigma \tag{1}$$

where r_{ij} is the distance between the sites i and j and σ is the collision diameter. Packing density, φ, (or equivalently volume fraction) is defined as

$$\varphi = \frac{V_{ch}}{V} = \frac{\frac{4}{3}\pi\left(\frac{\sigma}{2}\right)^3 n}{V} = \frac{\pi}{6}\frac{n}{V}\sigma^3 \tag{2}$$

where V is the total volume of the simulation cell, V_{ch} is the volume occupied by the chain molecules and n is the total number of hard spheres in the system. All simulations were executed in a cubic box with periodic boundary conditions applied in all three dimensions. Two different (polydisperse) athermal systems were studied: (i) 100 chains with an average of 12 hard spheres per chain ($N_{av} = 12$), and (ii) 50 chains with an average of 24 hard spheres per molecule ($N_{av} = 24$). Since both systems consisted of exactly the same total number of hard spheres ($n = 1200$) they were characterized by identical box dimensions (see eq 2, with σ being constant in all simulations).

As will be explained in more detail in section III, some of the chain-connectivity altering (and localized) moves, applied in the course of the present work, require a finite degree of polydispersity in order to function (a feature similar to that of the end-bridging (EB) move for atomistic systems as described analytically in refs 50 and 61). Consequently, all polydisperse simulations were cast in the $N_{ch}nVT\mu^*$ ensemble, where N_{ch} is the total number of chains and μ^* is the spectrum of relative chemical potentials of all chain species except two, which are taken as reference species (the derivation of the reduced chemical potential spectrum for various molecular length distributions can be found in ref 50 and is briefly described in the Appendix). In the present work, all chain lengths were allowed to fluctuate uniformly around an average value (N_{av}) within the closed interval $[N_{av}(1 - \Delta), N_{av}(1 + \Delta)]$, where Δ is the half-width of the molecular length distribution divided by N_{av}. In the limit of very long chains Δ is related to the polydispersity index, I, through $I = 1 + \Delta^2/3$.[61] In all simulations, the reduced half-width was set equal to $\Delta = 0.5$, which practically means that the 100- and 50-chains systems consisted of molecules lying between minimum and maximum lengths of 6 and 18 ($N_{av} = 12$) and of 12 and 36 ($N_{av} = 24$), respectively. For packing densities in the intermediate regime ($0.20 \leq \varphi \leq 0.50$) simulations were also conducted on strictly monodisperse systems (in the canonical (NVT) ensemble) to ensure that the applied degree of polydispersity does not affect average chain size and local packing (as already shown in ref 62 for atomistic analogs). The inclusion of chain-connectivity altering moves additionally required the adaptation of a small (but nonzero) fluctuation of all bond lengths so as to achieve the optimum algorithmic performance. More details are presented in section IV.

Initial, (dilute) nonoverlapping configurations for both systems were borrowed from equilibrated trajectories of monodisperse polyethylene systems (C_{12} and C_{24}) in united-atom representation with constant bond lengths[51,62] corresponding to a volume fraction approximately equal to $\varphi \approx 0.055$ for hard-sphere chains (where σ is taken equal to the bond length). For the system with smaller chains ($N_{av} = 12$) initial structures were additionally generated by splitting all molecules of the system with longer chains ($N_{av} = 24$) so as to produce twice the number

of chains all with half lengths (compared to the original ones). In practice for any given hard-sphere system, any set of N_{ch} freely jointed chains, with each bearing an average of N_{av} hard-spheres, can be trivially decomposed into a larger set of N_{ch}' chains with N_{av}' molecular lengths under the obvious condition that $N_{ch}'N_{av}' = N_{ch}N_{av}$.[63] In contrast, merging athermal chains into smaller ($N_{ch}' < N_{ch}$) assemblies of larger molecules ($N_{av}' > N_{av}$) is not straightforward, especially for systems of long chains bearing a limited number of chain ends.

In order to efficiently reduce the computational time required, the simulation cell is divided in a number of subcells, each with dimensions slightly larger than the collision diameter σ. In every attempted MC move the new position(s) of the hard sphere(s) is (are) tracked, and distance checks for overlaps are solely limited on hard spheres that belong on one of the 27 reference subcells. As will be described in more detail in section IV, the overlap subcells, defined here, serve also as reference cubes (called "connectivity-neighbor cells") for the rapid creation of neighbor lists used during the initialization of the chain-connectivity altering algorithms.

III. Simulation Details

The new MC suite for the generation and relaxation of dense systems of freely jointed athermal chains consists of moves falling into three major categories: (i) "Localized" MC algorithms involving the displacement of a single sphere positioned in either the inner segment (flip[64]), or the ends (rotation,[48] reptation,[55,56,65] intermolecular reptation[66]) of a chain, (ii) "localized" MC move involving the (energetically biased) reconstruction of a whole end-segment of spheres (continuum configurational bias (CCB)[37,57,58,67−71]), and (iii) chain-connectivity altering moves either affecting a pair of chains (in a fashion similar to the end- (EB)[50,61,72] and double- (DB)[51,62,66] bridging algorithms for atomistic chains) or involving rearrangements within a single chain (like the intramolecular end-bridging (IEB) or the intramolecular double-rebridging (IDR)[51,62])

More algorithmic details about the aforementioned MC sampling moves, applied on atomistic polymer systems, can be found in the analytical reviews of refs 71, 73, and 74.

A key feature of the present MC suite is that all localized moves (flip, rotation, reptation, and intermolecular reptation) are executed in a continuum configurational bias pattern in the spirit of the original CCB algorithm. According to the CCB scheme in the attempted regrowth step of any localized move the displaced hard sphere (or succession of hard spheres in the case of the original CCB) has n_{dis} different positions to choose from, each of them obtained from a different (randomly selected) torsion angle. The bias introduced in the selection of a candidate position is removed by performing the transition in the reverse order in a completely analogous way. More details about the original CCB scheme can be found in refs 37, 57, 58, and 67−71, while an application of the configurational-biased reptation in atomistic polymer models is presented in ref 75. To distinguish between different executions of the same algorithm, in the rest of the manuscript, we will use the term "bias" in the notation of a move to state that it is formulated in a CCB pattern (that is $n_{dis} > 1$, in contrast to the conventional "bare" form where $n_{dis} = 1$).[76] Another important aspect of the present modeling approach is that the number of attempted trial positions, n_{dis}, for each biased move does not remain constant in all simulations but rather increases (significantly) with increasing packing density as reported in Table 1 (but remains constant with chain length). Again, to distinguish between the bias-MC scheme that employs variable n_{dis} depending on volume fraction and the more conventional one (where n_{dis} is constant, independent of packing density), we will adopt the term "adaptive-bias" to describe the former implementation.

Table 1. Number of Employed Trial Positions, n_{dis}, for the Adaptive Continuum Configurational Bias Execution of Local Monte Carlo Moves as a Function of Packing Density, φ, Where for a Given Volume Fraction n_{dis} Is Common between Different Types of MC Moves and Independent of Chain Length

φ	0.01	0.10	0.20	0.30	0.40	0.45	0.50	0.52	0.54
n_{dis}	1	5	5	5	10	20	40	40	40
φ	0.56	0.58	0.60	0.61	0.62	0.63	0.637[a]	0.639[b]	
n_{dis}	50	50	70	70	70	70	100	100	

[a] Densest simulated random structure of $N_{av} = 12$. [b] Densest simulated random structure of $N_{av} = 24$.

Regarding the incorporation of other advanced, intrachain algorithms involving the rearrangement of a whole succession of hard spheres through the bridging of a properly selected pair of spheres like the original ConRot[59] or the extended version[71] preliminary simulations revealed that they exhibit very poor performance (due to extremely low acceptance rates) at packing densities near or higher than the melting transition.

Identical performance issues, strongly related to very low acceptance rates near and above φ_M, plague the more sophisticated chain-connectivity altering moves that are also built round the trimer bridging of a properly selected pair of hard spheres (one of which should be a chain-end). In the original (and widely used) implementation of EB,[50,61] no configurational biasing is employed in the reconstruction of the triplet of displaced mers, thus for dense packings in the majority of the attempted EB moves all candidate geometrical configurations lead to energetic overlaps. For systems of freely jointed chains poor acceptance rate for EB is further caused by the geometrical construction of the trimer bridge since it entails the random selection of five bending angles that, in principle, cannot bridge the predator−prey pair if they lie far apart. Not surprisingly, both issues are even more severe for chain-connectivity altering moves that entail double trimer bridge reconstructions like the DB or IDR.[51,62,66,74] Consequently, in the original realizations of DB and IDR, algorithmic effectiveness diminishes at volume fractions slightly above φ_F. Solution to the problem of very low acceptance rates could be provided by casting the chain-connectivity altering moves in a min-map bias scheme[77] based on the bijective mapping strategy;[78] still, we cannot safely predict if such a scheme will be adequate for the generation and relaxation of random chain assemblies of hard spheres near the MRJ state.

In the next section we describe novel formulations of the existing chain-connectivity altering moves, specially designed to function on very dense systems of freely jointed, hard-sphere chains, which are not plagued by the aforementioned performance issues.

IV. Chain-Connectivity Altering Moves for Freely Jointed Chains of Hard Spheres

IV.1. Simplified End-Bridging (sEB). The first move of the chain-connectivity altering class of MC algorithms is termed "simplified end-bridging" (sEB) and as its title suggests it constitutes a modification (simplification) of the original end-bridging[50] with the distinctive feature of not involving any hard sphere displacement (a related chain connectivity-altering algorithm has been introduced by Bunker and Duenweg for the simulation of bead−spring model chains).[79] The schematic of the sEB move is shown in Figure 1. As depicted in the left part of Figure 1 in the beginning of the move an end-sphere, *i* ("predator"), belonging to chain *ich*, is tangent, within a

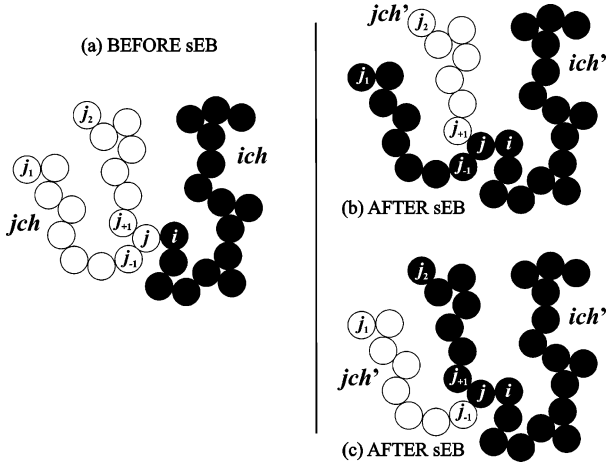

Figure 1. Schematic representation of the simplified end-bridging (sEB) move. Key: (a) initial configurations of the chains *ich* and *jch* before the application of the sEB move; (b, c): the two possible trial configurations of the new *ich*′ and *jch*′ chains after bonding spheres *i* and *j*.

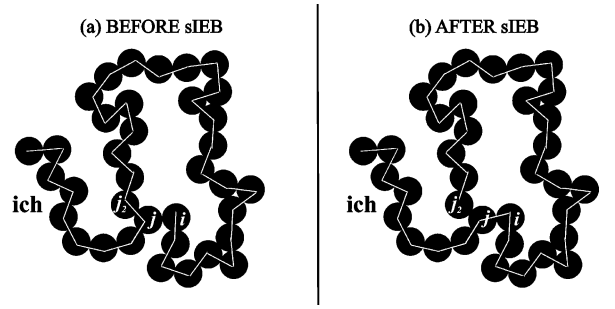

Figure 2. Schematic representation of the simplified intramolecular end-briding (sIEB) move. Key: (a) initial state of the chain where spheres *i* and *j* lie within a distance of $\sigma + \delta\sigma$; (b) final state after bonded spheres *j* and j_2 are detached and a new bond connects spheres *i* and *j*. Also shown is the contour length of the hard-sphere chain in the two states.

tolerance of $\delta\sigma$, to hard sphere *j* ("prey") belonging to chain *jch*. sEB proceeds in attempting to alter the connectivity of the participating *ich* and *jch* chains by treating *i* and *j* as bonded spheres based on two criteria: (i) the aforementioned proximity as *i* and *j* should lie within the $\sigma + \delta\sigma$ distance and (ii) at least one of the two possible rebridging combinations leads to new chains *ich*′ and *jch*′ with molecular lengths belonging to the closed interval $[N_{av}(1 - \Delta), N_{av}(1 + \Delta)]$ of the imposed chain-length distribution.

From the numerical point of view, the simulated athermal chains are not composed of strictly tangent spheres since a very small numerical tolerance in the bond length constraint must be used to test for promixity. In all simulations $\delta\sigma$ was set equal to $10^{-4} \times \sigma$, a value which is 2 orders of magnitude more stringent than the corresponding one ($\delta\sigma = 0.05$) used in refs 44 and 80. Our preliminary simulations with varying $\delta\sigma$ (also adopting a value that tends to zero, corresponding to strictly tangent spheres) confirmed previous findings[30] that sphere packing and chain dimensions, predicted by this model, are identical to the "pearl-necklace" model. The present value of $\delta\sigma$ was considered optimal as the adjustment to smaller $\delta\sigma$ only affected the performance of the sEB (since a decrease in $\delta\sigma$ shrinks the total number of hard-sphere pairs that can initiate a distinct sEB) while there was no detectable difference in the static properties (chain dimensions, bonded geometry and intersphere packing) of the modeled systems.

Table 2. Percentage Attempt Probabilities for Each Move Participating in the Monte Carlo Schemes Employed in the Present Work

move	adaptive-bias[a] CCAM	adaptive-bias[a] (no CCAM)	bias ($n_{dis} = 6$)	bare ($n_{dis} = 1$)
rotation	10.0	10.0	10.0	10.0
reptation	10.0	10.0	5.0	5.0
flip	34.8	25.0	30.0	30.0
CCB[b]	20.0	30.0	30.0	30.0
intermolecular reptation	25.0	25.0	25.0	25.0
sEB	0.10	0	0	0
sIEB	0.10	0	0	0

[a] The number of trial positions, n_{dis}, for the biased implementation of the localized moves depends on packing density, φ, and is reported in Table 1. [b] See ref 76.

As shown in Figure 1a given that *i* and *j* are within the bridgeable $\sigma + \delta\sigma$ distance the move can be executed in a maximum of two combinations: in the first (Figure 1b) the part of *jch* with the succession of spheres from j_{-1} to the free end j_1 gets attached to chain *ich* and thus becomes part of the newly formed *ich*′, while what remains as the shrunk *jch*′ is the segment of *jch* from spheres j_{+1} to j_2. In the second possible pattern (shown in Figure 1c) it is the segment of *jch* from j_{+1} to j_2 that is now appended to *ich* to form the grown *ich*′, while the updated *jch*′ is limited to the sequence of spheres j_1 ... j_{-1}. As clearly shown in both patterns of Figure 1, parts b and c, successful completion of the sEB leads to an increase (in the number of spheres) of one participating chain (where the "predator" end-sphere belongs to, that is *ich*) while the other one (*jch*) gets shorter since the total number of atoms in the two assemblies has to remain the same as in the original state. It is obvious that inclusion of sEB in the mix of MC algorithms has the side effect of introducing polydispersity in chain lengths. We described in detail in section II and in the Appendix that the effect of polydispersity can be fully controlled by a careful selection of a spectrum of relative chemical potentials of all chain species present in the system. Monodisperse samples can be effectively modeled through another set of chain-connectivity altering moves involving the rebonding of two pairs of spheres, albeit at a higher computational cost. It is established that the decorrelation rate, achieved by the MC scheme, for systems of monodisperse molecules is quite slower than the one for polydisperse analogs of the same average chain length.[51,62,74] Although the generation and relaxation of strictly monodisperse configurations of dense athermal systems are equally desirable (and they constitute the focus of present modeling studies), through polydisperse MC simulations one is able to collect a wealth of information about structure, packing and chain dimensions as a function of chain length from a single trajectory. Additionally, MC simulations on strictly monodisperse athermal samples at intermediate packing densities revealed that there is no appreciable effect of the implied polydispersity ($I = 1.083$) on the average structural and packing features (same qualitative trends on the effect of polydispersity on static properties are also reported for atomistic counterparts in refs 51, 62, and 74).

sEB proceeds as follows: initially, the overlapping cells are detected for all chain ends existing in the simulation box and successively we identify all intermolecular neighbors that belong to one of the 27 reference subcells (cell of the reference end-sphere plus the 26 adjacent ones). Distance checks are performed so as to identify all bridgeable pairs that lie within the $\sigma + \delta\sigma$ range. If the proximity criterion is fulfilled for at least one interchain neighbor then, based on the relative position of *j* in chain *jch* and the original chain lengths $N(ich)$ and $N(jch)$, the lengths of the new chains ($N(ich')$ and $N(jch')$) are calculated

Table 3. Average CPU Time (in Seconds) per 10 Million Steps (Corresponding to One Trajectory Frame) for the Various MC Schemes Employed in the Present Work, Where All Reported Times Correspond to Runs on an Intel Pentium IV Processor (2 MB RAM, 3.0 GHz) and Parameters for Each MC Scheme Are Given in Tables 1 and 2

φ	bare CPU time (s)	bias CPU time (s)	adaptive-bias CPU time (s)	adaptive-bias, CCAM CPU time (s)
0.30	40	220	170	190
0.40	33	170	250	280
0.50	30	150	900	1000
0.60	27	130	1300	1400

for both combinations of the sEB algorithm. If at least one of the two sEB patterns leads to feasible new configurations then the "predator" end-sphere, *i*, along with its "prey" companion-sphere, *j*, are added (along with their feasible combination(s)) in the active set of pairs that can initiate a sEB-based sampling transition. A trial sEB move begins through the random selection of a chain end *i* (that participates in at least one pair of "predator−prey" spheres). If the sEB-related lists are empty in the initialization step then the move is automatically rejected. Out of all bridgeable candidates of *i*, $n_{sEB}(i)$ one is selected randomly along with a sEB combination (in the case that both are available). Chains *ich′* and *jch′* are further re-formed with their connectivity fully defined by the selected pattern. For the new *jch′* we identify the new end, j_{end} (which corresponds to either the j_{+1} (Figure 1b) or the j_{-1} (Figure 1c) sphere depending on the applied sEB combination). In the final stage, since the move does not involve any hard-sphere displacements it is accepted or rejected according to the following ratio, which constitutes a simplification of the original acceptance criterion of EB:

$$P_{acc}^{sEB}(\text{old} \rightarrow \text{new}) = \min\left[1, \frac{w(\text{new} \rightarrow \text{old})}{w(\text{old} \rightarrow \text{new})}\right] = \min\left[1, \frac{\dfrac{1}{n_{sEB}(j_{end})}}{\dfrac{1}{n_{sEB}(i)}}\right] \quad (3)$$

where notations "old" and "new" denote the initial and final states, respectively, and *w* denotes the appropriate weighting factor for the attempted transition, being reciprocal to the total number of sEB neighbors for the reference chain-end (corresponding to sphere *i* for the forward (old → new) transition and to sphere j_{end} for the reverse (new → old) one). In contrast to its atomistic counterpart (EB), sEB does not invoke the trimer-bridging geometrical procedure[50,59] nor does it execute a series of screening procedures to discard candidate solutions,[61] and most importantly it is not engaged in any kind of energetic calculations (overlap detections for athermal chains) entering the modified Metropolis acceptance criterion. Consequently, the average computational (CPU) time is considerably smaller, as practically the only time-consuming calculations involve the creation of the sEB-based neighbor lists in the forward and reverse transitions (a procedure which is greatly enhanced by the existence of the connectivity-neighbor subcells). On the other hand, in its present formulation, the applicability of sEB is restricted to chain systems dictated exclusively by those types of potential interactions that allow the close proximity (tangency) of intermolecular neighbors (hard-spheres, square-well potential etc.).

IV.2. Simplified Intramolecular End-Bridging (sIEB). Figure 2 depicts the schematic of the "simplified intramolecular end-bridging" (sIEB) which, as its title suggests, constitutes the intramolecular (single-chain) analog of the sEB algorithm. Again, it is inspired by the intramolecular end-bridging (IEB), developed for the simulation of atomistic polymer chains, where connectivity rearrangement is confined solely to a single macromolecule.[74] As shown in Figure 2a, in the original state the "predator" free-end, *i*, of chain *ich* lies within the $\sigma + \delta\sigma$ bridgeable distance from internal "prey" site *j* that belongs in the same chain. As shown in the right part of the scheme after the trial sIEB-based transition, bonded spheres *j* and j_2 become separated, while a new bond is formed between spheres *i* and *j*. This intramolecular rebonding leaves sphere j_2 as the newly formed end of *ich*. The change afforded in the chain-connectivity by the sIEB move can be easily tracked by following the contour lengths of the chain in the original and final states as shown in Figure 2. Given an internal sphere, *j*, and a chain end, *i*, which fulfill the proximity (distance) criterion there is a single pattern that sIEB can be executed (the other combination leads to the scission of the original chain in two segments). The second criterion of sEB regarding restrictions imposed on molecular length is, by construction, always fulfilled in sIEB. The move proceeds further in a completely analogous way to its intermolecular counterpart (sEB), by identifying all "predator−prey" pairs that can initiate a sIEB move. For each chain-end, we identify (by checking again over all 27 overlap cells) all intramolecular neighbors, separated by at least three bonds from

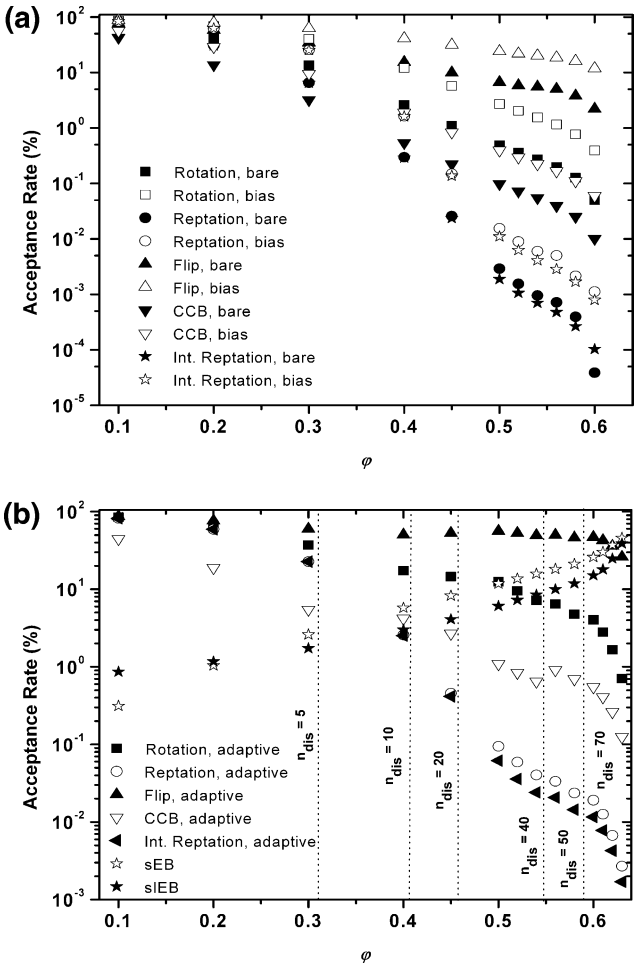

Figure 3. Percentage acceptance rates for the Monte Carlo moves included in (a) the bare ($n_{dis} = 1$) and bias ($n_{dis} = 6$) schemes and (b) the "adaptive-bias, CCAM" suite as a function of packing density, φ, from simulations of freely jointed chains of hard spheres ($N_{av} = 24$). Vertical dotted lines in part b denote the regimes of constant number of trail configurations, n_{dis}, for the adaptive scheme (see manuscript and Table 1 for details).

Table 4. Total Simulation Time (in Billions of MC Steps) of the "adaptive-bias, CCMA" MC Scheme for the Simulated $N_{av} = 12$ and 24 Chain Systems at Various Packing Densities, φ

	$\varphi =$ 0.10	$\varphi =$ 0.20	$\varphi =$ 0.30	$\varphi =$ 0.40	$\varphi =$ 0.45	$\varphi =$ 0.50	$\varphi =$ 0.52	$\varphi =$ 0.54	$\varphi =$ 0.56	$\varphi =$ 0.58	$\varphi =$ 0.60	$\varphi =$ 0.61	$\varphi =$ 0.62	$\varphi =$ 0.63	$\varphi =$ 0.635	$\varphi =$ 0.639
$N_{av} = 12$	20	20	20	20	20	20	30	30	40	100	140	140	200	180	100	
$N_{av} = 24$	20	20	20	20	20	20	30	30	40	40	100	140	160	170		100

the reference end-sphere, that lie within $\sigma + \delta\sigma$. The tolerance, $\delta\sigma$, is set at exactly the same value as the tolerance used in the sEB move ($10^{-4} \times \sigma$). A random selection of one of the "active" (for sIEB) chain-ends, i, takes place, followed by the random selection of one of its sIEB-neighbors, j, out of all possible pairs, $n_{sIEB}(i)$. The trial move concludes by identifying all sIEB neighbors of the new chain-end, j_2, $n_{sIEB}(j_2)$ in the final state. Finally the trial move is accepted or rejected according to

$$P_{acc}^{sIEB}(\text{old} \rightarrow \text{new}) = \min\left[1, \frac{w(\text{new} \rightarrow \text{old})}{w(\text{old} \rightarrow \text{new})}\right] = \min\left[1, \frac{\frac{1}{n_{sIEB}(j_2)}}{\frac{1}{n_{sIEB}(i)}}\right] \quad (4)$$

In comparison to the sEB, the intramolecular version (sIEB) is more general as it can be applied on (i) strictly monodisperse athermal systems and (ii) very dilute chain packings where the proximity condition between intermolecular neighbors is rarely satisfied.[81] On the other hand, its drawbacks can be summarized as that (a) it applies connectivity alternations within a single chain (thus the efficiency in modifying the long-range characteristics of an accepted sIEB is half that of a successful sEB), and (b) for a given pair of spheres it can be executed in a single pattern leading to fewer combinations that may produce "shuttling" effect[62] (i.e., successive transitions that annihilate each other by performing a transitional loop (old → new, new → old).

IV.3. Mix of Monte Carlo Moves. The proposed MC suite for the simulation of dense packings of athermal chains is composed of the following moves: (i) adaptive-bias reptation, (ii) adaptive-bias rotation, (iii) adaptive-bias intermolecular reptation, (iv) adaptive-bias flip, (v) adaptive continuum configurational bias, (vi) simplified end-bridging (sEB), and (vii) simplified intramolecular end-bridging (sIEB). For the localized biased moves the implemented variable values for n_{dis} as a function of packing density are reported in Table 1. The attempt probabilities for each move, independent of MC protocol, remained unaltered for the whole range of volume fractions and chain lengths studied here and they are reported in Table 2. The only exception to the previous statement was the simulation of very dilute systems ($\varphi < 0.10$) where sEB was proven inefficient in practice, because of the very sparse set of pairs that could initiate the move. For these systems, sEB was excluded from the MC suite and its proportion of moves was distributed equally between sIEB and CCB (both being very efficient for dilute systems). In the rest of the manuscript the notation "adaptive-bias, CCAM" (where CCAM stands for chain-connectivity altering move) is adopted to describe the new MC scheme. The proposed scheme is compared against other MC suites that (a) exclude the usage of CCAMs but retain the adaptive bias pattern of the localized moves (termed "adaptive-bias", (b) exclude the usage of CCAMs and implement a conventional bias form for the localized moves ("bias" with constant $n_{dis} = 6$), and (c) exclude CCAMs and adopt a bare form for all localized moves ("bare" with $n_{dis} = 1$). As expected, as the complexity of the MC scheme increases so does the average CPU time consumed per MC step. In Table 3, the average CPU time per 10 million MC steps (which correspond to 1 trajectory frame) is reported for the bare, bias, adaptive-bias and adaptive-bias, CCAM schemes. Since the CPU time depends on both a large set of different simulation parameters (attempt probability, acceptance rate, number of trial positions, number of reconstructed hard spheres, etc.) and on the level of optimization applied on the MC code (incorporation of neighbor cells, overlap cells etc.) in the rest of the manuscript we present all results in "raw" MC steps. To study the effect of polydispersity, a different mixture of the adaptive-bias, CCAM scheme was employed for the simulation of strictly monodisperse systems with the intermolecular reptation and sEB moves being excised from the MC scheme as both algorithms impose polydispersity in chain lengths.

Parts a and b of Figure 3 show the percentage acceptance rates as a function of packing density for each individual move participating in the bare (Figure 3a), bias (Figure 3a), and adaptive-bias, CCAM (Figure 3b) *NVT* MC schemes (serving for the equilibration part of the simulation). Given that for the adaptive bias schemes all localized moves are executed in exactly the same manner whether chain-connectivity moves are included in the mix or not, their acceptance rates are identical within the statistical error (as will be shown in the following sections a similar statement for the corresponding sampling efficiency of localized moves, in the presence or absence of CCAMs, is not valid). Two important conclusions can be drawn by analyzing the data shown in Figure 3: first, the bare scheme is rendered practically inefficient at volume fractions greater than $\varphi > 0.45$ as the acceptance rates of all moves (except flip) fall below 1%, while the conventional bias scheme exhibits similar behavior but with a prolonged efficiency that reaches packing densities up to $\varphi \approx 0.54$. In both cases, reptation moves (both intra- and intermolecular variants) are mostly plagued by the increment of density, not surprisingly as reptation affords sphere displacements that are much more extended that the ones caused by successful flips or rotations.

Before even applying any equilibration measures for the simulated trajectories, by evaluating the acceptance rate trends for the bare and bias MC schemes, it is clear that both are practically inept in generating and equilibrating dense structures close to the MRJ state even for small chain lengths. A second important finding is that the novel scheme, built around the adaptive-bias implementation, seems to significantly enhance the acceptance rates of all localized moves at quite higher densities. For example the adaptive-bias flip begins with an acceptance rate of approximately 87% for dilute systems ($\varphi = 0.10$) and ends up to an acceptance rate of 26% at $\varphi = 0.63$, quite close to the MRJ state. For the reptation moves at $\varphi = 0.60$, acceptance rates were found to be 4×10^{-5}, 1×10^{-3}, and 2×10^{-2} for the bare, bias, and adaptive-bias schemes, and the performance gap gets wider as the systems become denser. Obviously, at the close vicinity of the MRJ state it is expected that the acceptance rate of all local moves, even when cast in an adaptive-bias fashion, diminishes as spheres get jammed. This behavior is already established by tracking the "rattler" spheres for monatomic hard-sphere assemblies[25] and the "flipper" analogs for chain random packings.[60]

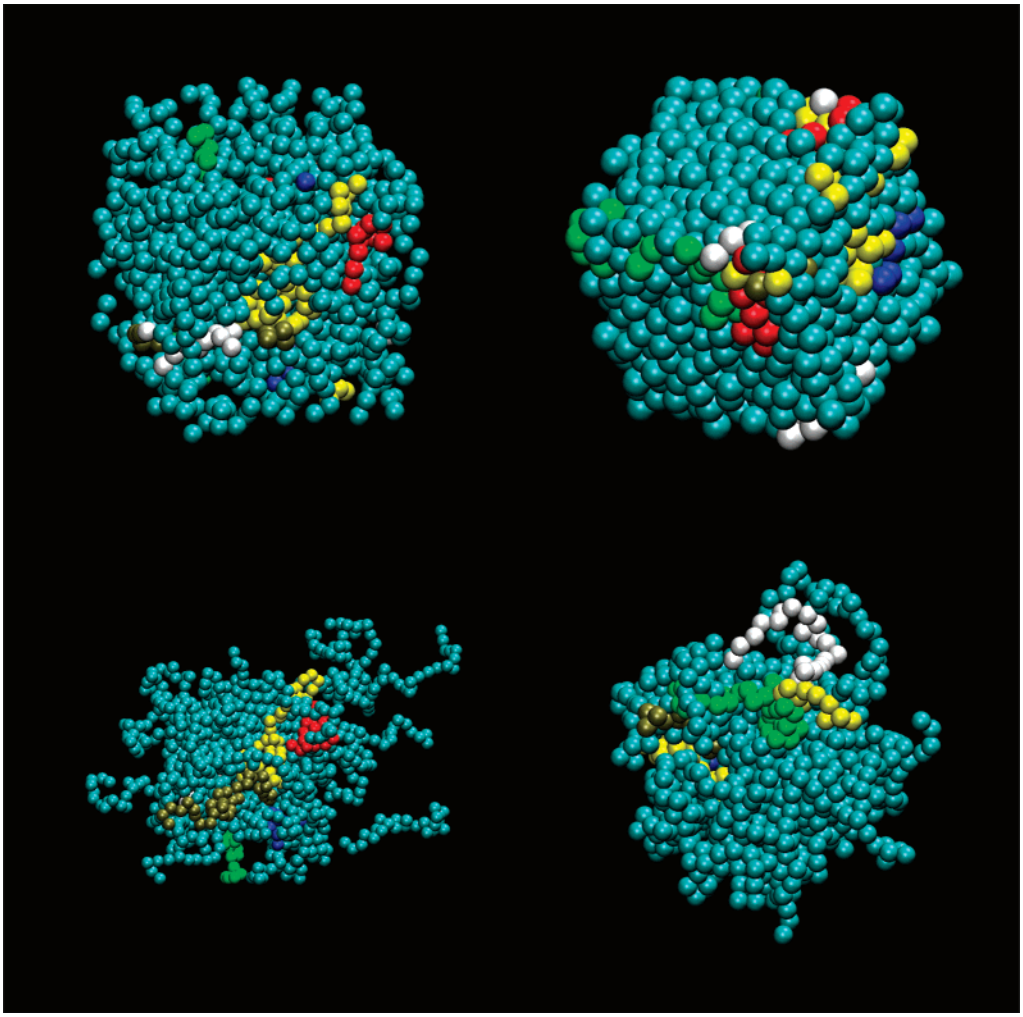

Figure 4. Simulation snapshots of packings of freely jointed chains of hard spheres (top) in box coordinates and (bottom) fully unwrapped in space for (i) a dilute system ($\varphi = 0.10$) and (ii) a system near the MRJ state ($\varphi = 0.639$) with $N_{av} = 24$. Eight, randomly picked chains are sketched in different colors for visualization purposes.

The newly introduced CCAMs (sEB and sIEB) exhibit a unique and striking behavior: in sharp contrast to every available MC algorithm their acceptance rates increase with increasing packing density. Although at a first glance this feature appears as a "paradox" its explanation is quite straightforward based on the algorithmic details provided in section IV. Both CCAMs do not involve any kind of sphere displacement; therefore they are not plagued by rejections caused by hard-sphere overlaps. On the basis of eqs 3 and 4, the only terms entering the acceptance criteria of sEB and sIEB are the weighting factors related to the number of bridgable neighbors around the reference sphere. By construction, even for dilute systems ($\varphi \geq 0.10$) there is always a limited (but nonzero) set of pairs that can initiate sEB or sIEB moves. Preliminary simulations on very dilute systems ($\varphi \leq 0.01$) suggested that only then chains are practically isolated, thus the proximity condition between spheres belonging to different chains is rarely fulfilled. It is in this range of densities that sEB is practically inefficient (in contrast, there still exists an appreciable number of pairs that can initiate a sIEB move).[81] As packing density increases, (i) chains are packed more closely together (enhancing the efficiency of sEB) and (ii) they tend to coil as their dimensions get notably collapsed (enhancing the efficiency of sIEB).

V. Results

V.1. Creation of Dense Structures of Athermal Chains. The first challenge encountered in the simulation of dense random assemblies of freely jointed chains of hard spheres is the generation of the simulation cell with overlap-free coordinates for all existing hard spheres. It is obvious that the generation problem intensifies as we reach volume fractions in the vicinity of the MRJ state. In the present work, we adopted a "box shrinkage" algorithm based on the MC scheme presented in section IV. For this purpose, we have included a modified version of a typical volume fluctuation algorithm where only isotropic shrinkages (and not expansions) of the simulation box are attempted. During a trial cell reduction, all chains present in the system are affinely repositioned based on the original distance between their end and the box origin and the amplitude of the attempted reduction, δl. Whereas the bonded geometry (bond lengths, bending and torsion angles) and connectivity in each chain remain unaltered during a volume fluctuation, all intermolecular distances are changed leading possibly to hard-sphere overlaps. For dense systems, δl should be very small; otherwise, all trial volume reductions are rejected. In addition, each attempted box shrinkage leads to a recompilation of all overlap subcells, a procedure which is computationally very expensive; the average CPU time allocated in an attempted volume reduction is larger, by 1 order of magnitude, than the average time needed for the execution of the moves included in the "adaptive-bias, CCAM" scheme. Key components for the efficient application of the volume reduction are primarily the judicious selection of the δl parameter and the attempt frequency

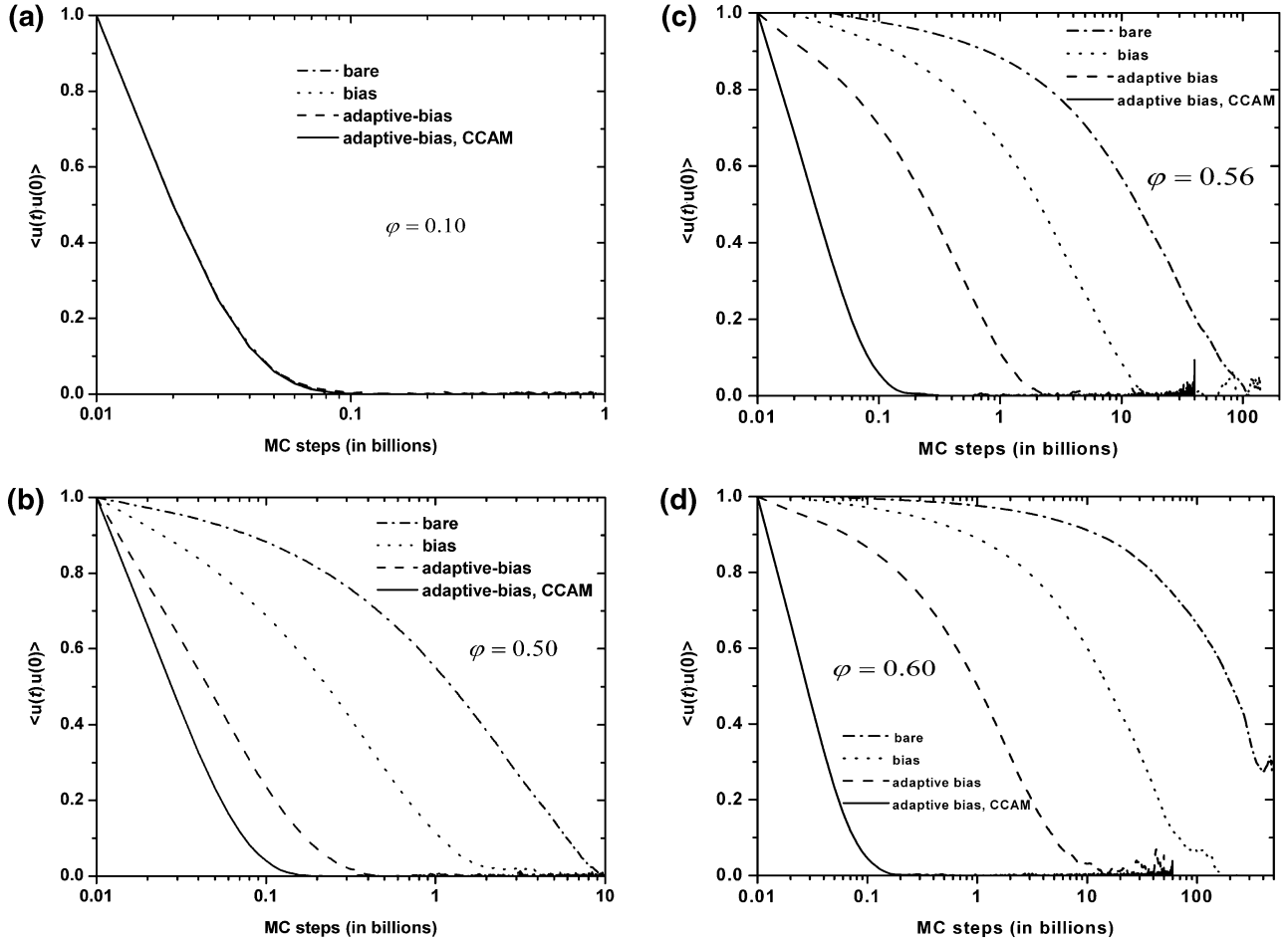

Figure 5. Evolution of the orientational autocorrelation function of the end-to-end unit vector, $\langle \mathbf{u}(t)\mathbf{u}(0)\rangle$, as a function of CPU time (in MC steps) for the (i) bare ($n_{dis} = 1$) [dash-dot line], (ii) bias ($n_{dis} = 6$) [dot line], (iii) adaptive bias [dash line], and (iv) adaptive-bias CCAM MC [solid line] schemes in log-linear coordinates. Reported simulation results are collected for the $N_{av} = 24$ system at packing densities: (a) $\varphi = 0.10$, (b) $\varphi = 0.50$, (c) $\varphi = 0.56$, and (d) $\varphi = 0.60$.

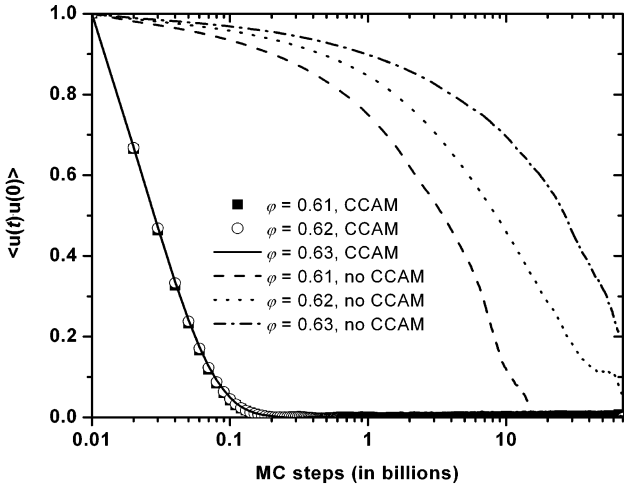

Figure 6. Evolution of the orientational autocorrelation function of the end-to-end unit vector, $\langle \mathbf{u}(t)\mathbf{u}(0)\rangle$ as a function of CPU time (in MC steps) for the (i) adaptive-bias, CCAM and (ii) adaptive-bias schemes as obtained from MC simulations on $N_{av} = 24$ at (i) $\varphi = 0.61$, (ii) $\varphi = 0.62$, and (iii) $\varphi = 0.63$ packing densities.

of the volume fluctuation. The latter was constant throughout the whole series of simulations with one volume reduction attempted every 1000 steps of $NVT-$MC moves. Too frequent attempts of box shrinkage may lead to sharp decline in its acceptance rate especially for dense systems, as the system should undergo structural rearrangements to be able to accommodate the overlap-free distortion of all intermolecular distances. The fraction of the cell fluctuation, δl, is the most critical factor for the successful application of the shrinkage algorithm: for a given density, too large a value will eventually lead to a large increase of hard-sphere overlaps and every trial will be rejected, while too small a value implies very small steps toward the desired packing density, thus increasing the computational time for the system generation. In our simulations, we have selected a δl value which allows a high acceptance rate (>90%) for intermediate densities ($\varphi < 0.60$) and a reasonable one (≈50%) for denser structures ($\varphi \geq 0.60$). Apparently, as we approach the MRJ state ($\varphi \approx 0.639$), the acceptance rate of the volume reduction diminishes. Through extensive preliminary simulations the optimum values for δl were set at

$$\begin{aligned} \delta l &\approx 10^{-4} \times \sigma, \quad 0.01 \leq \varphi \leq 0.40 \\ \delta l &\approx 10^{-5} \times \sigma, \quad 0.40 < \varphi \leq 0.58 \\ \delta l &\approx 10^{-6} \times \sigma, \quad 0.58 < \varphi \leq 0.62 \\ \delta l &\approx 10^{-7} \times \sigma, \quad 0.62 < \varphi < \varphi_{MRJ} \end{aligned} \tag{5}$$

It is clear that even in its most efficient implementation the proposed volume reduction algorithm needs significant computational time to reach densities near the MRJ state. In particular, it was found that the required simulation time to transit gradually from very dilute ($\varphi \approx 0.055$) to dense structures ($\varphi = 0.63$) is comparable to the CPU time needed to reach the

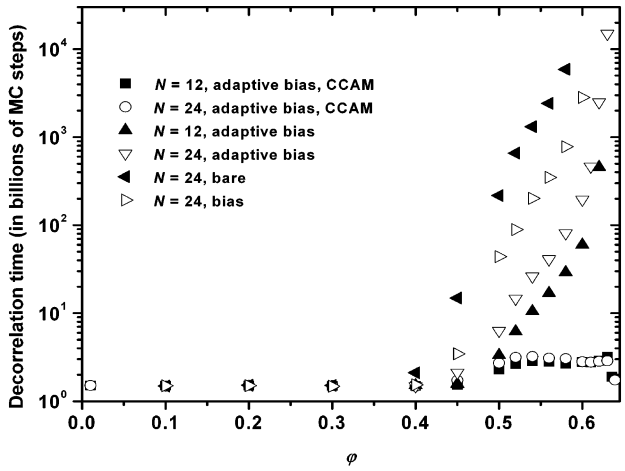

Figure 7. Dependence of the total decorrelation time, t_c, of the orientational autocorrelation function of the end-to-end unit vector on volume fraction, φ, as obtained from *NVT* MC simulations using the adaptive-bias and adaptive-bias, CCAM schemes on $N_{av} = 12$ and 24 systems. Also shown are corresponding simulation data from application of the conventional bare and bias schemes on the $N_{av} = 24$ system.

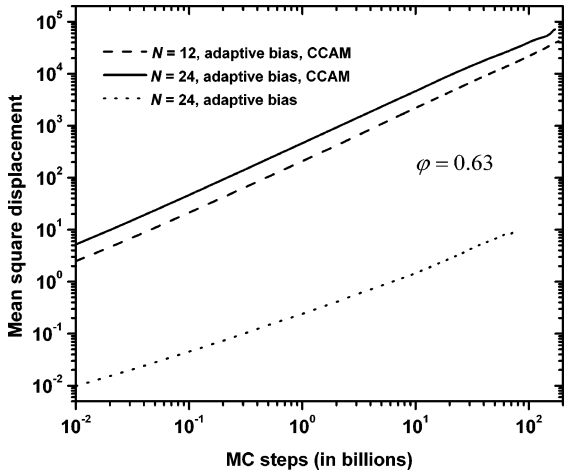

Figure 8. Center-of-mass mean-square displacement, averaged over all chains, as a function of MC steps, in logarithmic scale, for $N_{av} = 12$ and 24 as obtained from *NVT* simulations at $\varphi = 0.63$ using the adaptive-bias and adaptive-bias, CCAM schemes.

densest simulated random chain assembly ($\varphi = 0.639$ for $N_{av} = 24$) starting from a configuration at $\varphi = 0.63$. The computational time required for the whole shrinkage procedure is on the order of 3 months (in real time) executed in an Intel Xeon processor at 1.8 GHz. It must be noted that the CPU time consumed for the generation procedure was almost identical for the $N_{av} = 12$ and 24 systems. Since both athermal systems were characterized by the same total number of hard spheres ($n = 1200$) and accordingly by identical box dimensions at a given volume fraction (see eq 2), it can be concluded that the generation algorithm scales as N^0 for systems characterized by different chain lengths (N) but same total number of hard spheres (n). On the other hand, following the general trend of a typical volume fluctuation move, the box shrinkage becomes far less efficient as box dimensions increase.

After the successful creation of the initial (overlap-free) configuration at each volume fraction, exhaustive *NVT*−MC simulations are initiated based on the "adaptive-bias, CCAM" scheme described earlier. A system configuration (including chain connectivity and coordinates for all hard spheres) along with algorithmic statistics for the applied MC moves are recorded every 10^7 MC steps. All employed packing densities

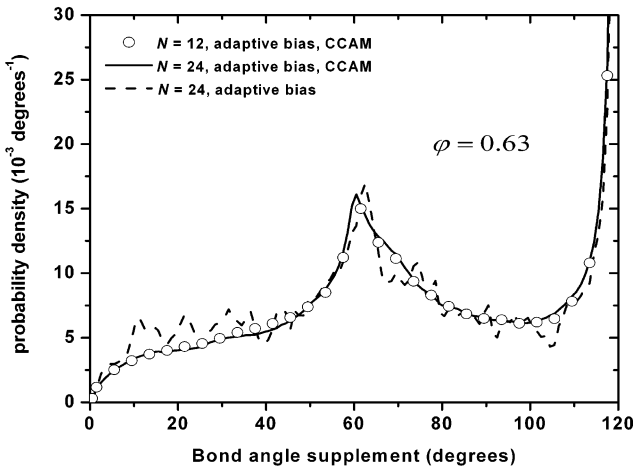

Figure 9. Distribution of supplement bond angle for the $N_{av} = 12$ and 24 systems at $\varphi = 0.63$ as obtained from MC simulations using the adaptive-bias and adaptive-bias CCAM schemes.

along with the total simulation time (in MC steps) for both chain systems ($N_{av} = 12$ and 24) are summarized in Table 4. Figure 4 depicts typical configurations of the simulation cell along with all athermal chains: (top) in box coordinates and (bottom) fully unwrapped in space for $N_{av} = 24$ (i) at $\varphi = 0.10$ and (ii) near the MRJ state ($\varphi = 0.639$).

V.2. Computational Efficiency. Static properties of freely jointed chains of hard spheres are dominated by a large spectrum of characteristic length scales starting from the bond length (along with bending and torsion angles) moving to the persistence length, ξ, and reaching the mean square radius of gyration, $\langle R_g^2 \rangle$, and the mean square end-to-end distance, $\langle R^2 \rangle$, of the chains. Before attempting to calculate these properties and study their dependence of volume fraction we need to establish the effectiveness of the proposed MC scheme by comparing it with the conventional suites listed in Table 2 using a number of commonly used and well-established measures. As a first quantity for the relaxation efficiency regarding the long-range system characteristics, we calculate the orientational autocorrelation function of the end-to-end unit vector, $\langle \mathbf{u}(t)\mathbf{u}(0) \rangle$, as a function of CPU time, t, for all chain lengths and packing densities. $\mathbf{u}(t)$ is the unit vector directed from one chain end to the other, and $\mathbf{u}(0)$ is the corresponding vector at reference time $t = 0$. CPU time, t, is calculated in MC steps and $\langle \rangle$ denotes averaging over all chains and recorded frames.

The faster $\langle \mathbf{u}(t)\mathbf{u}(0) \rangle$ drops to zero (decorrelates), the faster the system loses the trace of its original long-range conformation, i.e., the faster it relaxes with respect to the long-range characteristics. Parts a−d of Figure 5 present the evolution of $\langle \mathbf{u}(t)\mathbf{u}(0) \rangle$ as a function of CPU time for the $N_{av} = 24$ system as obtained from MC simulations using the bare ($n_{dis} = 1$), bias ($n_{dis} = 6$), adaptive-bias (see Table 1) and adaptive-bias, CCAM schemes (details about the attempt probabilities for every move in each mix are given in Table 2) at packing densities: (a) $\varphi = 0.10$, (b) $\varphi = 0.50$ (c) $\varphi = 0.56$, and (d) $\varphi = 0.60$. We should note here that all schemes were applied on exactly the same initial configuration at each volume fraction as obtained from the box-shrinkage procedure using the adaptive-bias, CCAM scheme (which is the only efficient MC scheme that can generate dense structures ($\varphi > 0.56$) within reasonable computational time). The behavior exhibited by each scheme and the associated comparison in equilibrating the long-range characteristics of the studied athermal systems deserves a thorough analysis. First, at the dilute regime represented by the volume fraction of $\varphi = 0.10$ (Figure 5a), it is clearly shown that all schemes manage

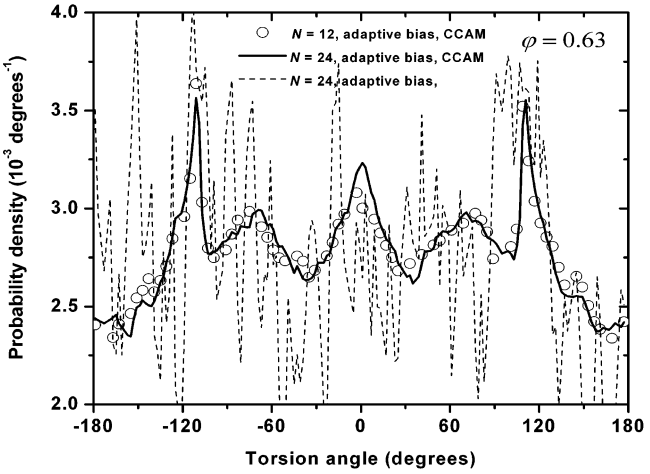

Figure 10. Same as in Figure 9 but for the torsion angle distribution (zero degrees correspond to the trans conformation).

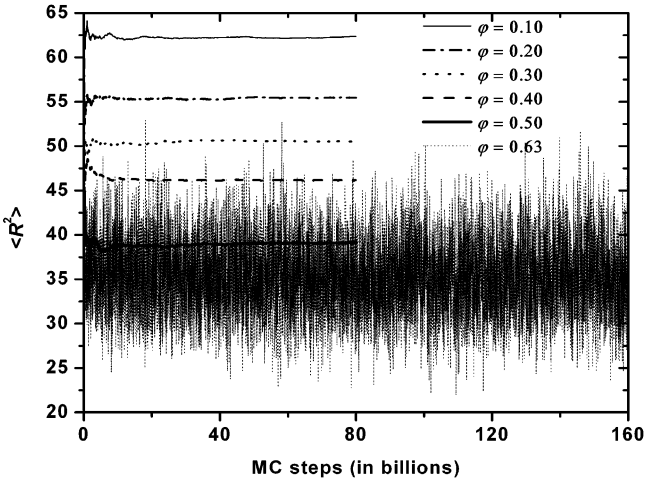

Figure 11. Running average value of the mean square end-to-end distance, $\langle R^2 \rangle$, as a function of MC steps as obtained from adaptive-bias, CCAM MC simulations on the $N_{av} = 24$ system at volume fractions of $\varphi = 0.10$, 0.20, 0.30, 0.40, 0.50, and 0.63. For the latter trajectory plot data correspond to the instantaneous value of $\langle R^2 \rangle$. Simulation times for all systems, except at $\varphi = 0.63$, are multiplied by a factor of 4 for visualization purposes (see Table 4 for the actual numbers).

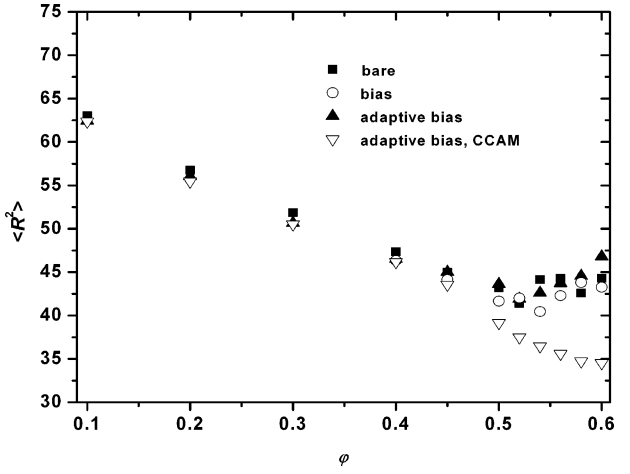

Figure 12. Dependence of the mean square end-to-end distance, $\langle R^2 \rangle$, on packing density, φ, as obtained from the (i) bare, (ii) bias, (iii) adaptive-bias, and (iv) adaptive-bias, CCAM scheme for the $N_{av} = 24$ system.

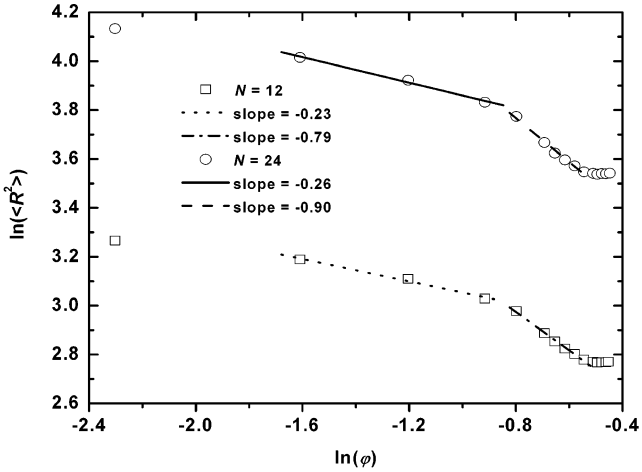

Figure 13. Natural logarithm of the mean square end-to-end distance, $\ln(\langle R^2 \rangle)$, as a function of the natural logarithm of packing density, $\ln(\varphi)$, for the $N_{av} = 12$ and 24 systems as obtained from MC simulations with the adaptive-bias, CCAM scheme. Also shown are lines that correspond to best linear fits on simulation data for different ranges of volume fractions.

to equilibrate the system at exactly the same rate as $\langle \mathbf{u}(t)\mathbf{u}(0) \rangle$ reaches zero after approximately 80 million MC steps (which translates in to roughly eight recorded MC frames). Given that (i) the average CPU time consumed per MC step is cheaper for the bare scheme and (ii) the mix that entails CCAMs is slightly more expensive than the others, the optimum (and reasonable) choice for the simulation of athermal systems characterized by chain lengths of this magnitude ($N = 24$) should logically be the direct implementation of the bare suite. The performance trend changes remarkably with increasing density as seen initially in Figure 5b: at $\varphi = 0.50$ (very close to the freezing transition for monatomic hard-sphere counterparts, $\varphi_F = 0.494$) the bare and bias schemes require almost 10 and 5 billion MC steps, respectively, for $\langle \mathbf{u}(t)\mathbf{u}(0) \rangle$ to drop to zero. According to the simulation data the adaptive-bias scheme is 1 order of magnitude more efficient than the conventional (bias) implementation and the full scheme (including the CCAMs) exceeds by almost 2 orders of magnitude the bare suite. Consequently, at volume fractions near φ_F the adaptive schemes (either with or without CCAMs) are already far more superior than the conventional analogs. At $\varphi = 0.56$, a volume fraction that lies beyond the melting transition ($\varphi_M = 0.545$), the efficiency of the bare scheme is practically nominal, requiring for the long-range relaxation a tremendous amount of around 100 billion MC steps (nearly the whole trajectory). The benchmark time of 20 billions MC steps is slightly better, but still totally inefficient for the conventional bias suite, while the adaptive implementation of the bias scheme requires a reasonable CPU time of around 2 billion MC steps. It is in this range of densities that the proposed CCAM-based adaptive-bias suite outperforms by a very wide margin all competitive suites by achieving relaxation in just 0.2 billion steps. The achieved relaxation time is 1 order of magnitude faster than the one without the CCAMs proving the critical role of the newly introduced advanced connectivity-altering moves in relaxing the long range characteristics of dense athermal systems. At $\varphi = 0.60$ (a packing density which is still quite below the MRJ state), as shown in Figure 5d, the two conventional schemes (bare and bias) are completely ineffective, since there is no hint of long-scale equilibration within the afforded simulation time. In parallel, the most advanced scheme (adaptive-bias, CCAM) shows its true potential at dense systems as it outperforms the adaptive bias scheme (without CCAMs) by approximately 2 orders of magnitude.

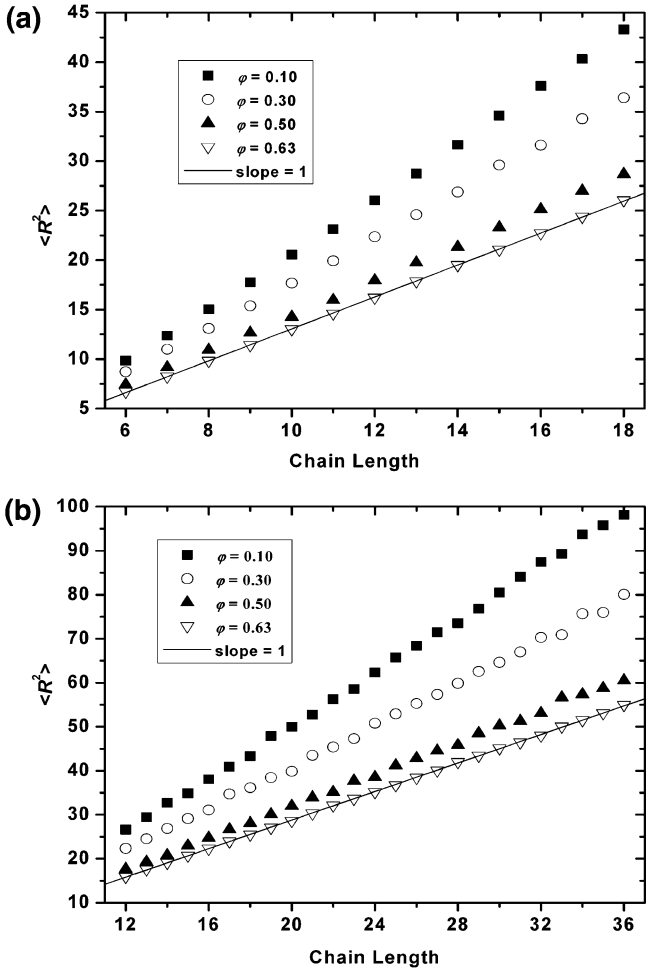

Figure 14. Mean square end-to-end distance, $\langle R^2 \rangle$, as a function of chain length, N, for various packing densities, φ, from adaptive-bias, CCAM MC simulations on (a) $N_{av} = 12$ and (b) $N_{av} = 24$ systems. Also shown are lines from best linear fits on simulation data for $\varphi = 0.63$.

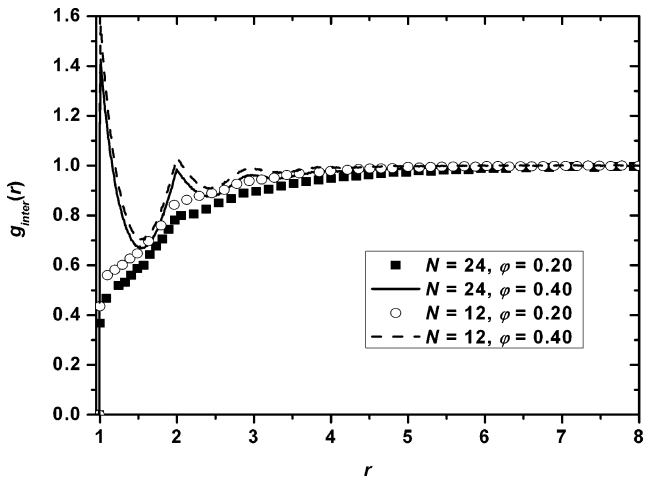

Figure 15. Intermolecular pair distribution function, $g_{inter}(r)$, as a function of radial distance, r, for the $N_{av} = 12$ and 24 systems at $\varphi = 0.20$ and 0.40.

Focusing the analysis on higher densities, even closer to the MRJ state, Figure 6 presents the evolution of $\langle \mathbf{u}(t)\mathbf{u}(0) \rangle$ as a function of MC steps for the adaptive-bias and adaptive-bias CCAM schemes for the $N_{av} = 24$ system at $\varphi = 0.61$, 0.62, and 0.63. As expected, the performance of the adaptive-bias scheme diminishes at an even higher rate as documented by

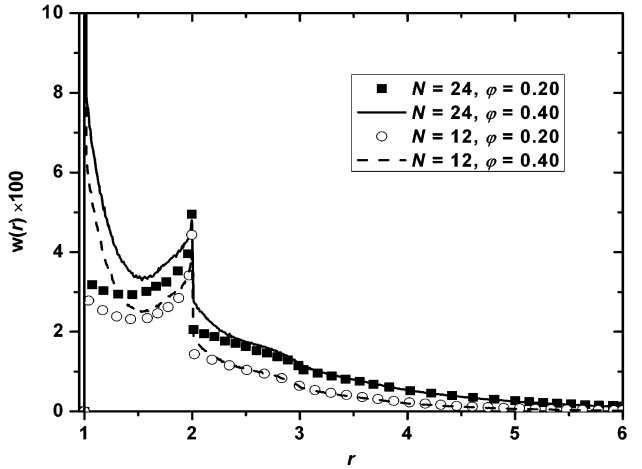

Figure 16. Same as in Figure 15 but for the intramolecular pair density function, $w(r)$.

the fact that for the two denser systems, chains remain trapped in their original configurations within the available simulation time. In sharp contrast, the efficiency of the MC scheme incorporating CCAMs is not affected by the increment in volume fraction as shown by the decorrelation $\langle \mathbf{u}(t)\mathbf{u}(0) \rangle$ curves of Figure 6, which coincide, within the statistical error, at all simulated densities.

The total decorrelation time, t_c(MC), for each employed MC scheme can be extracted by integrating the $\langle \mathbf{u}(t)\mathbf{u}(0) \rangle$ vs t curves (where t corresponds to CPU time measured in MC steps) and is shown in Figures 5 and 6. Calculated values of t_c (in billions of MC steps) as a function of packing density from application of the adaptive-bias and adaptive-bias, CCAM schemes on the $N_{av} = 12$ and 24 systems are reported in Figure 7. Also shown are corresponding benchmark data as obtained for the bare and bias schemes on the $N_{av} = 24$ system. It is evident that while in the low-density regime($0.10 \leq \varphi \leq 0.40$) all schemes are evenly efficient (thus there is no practical reason for adopting the complicated suites since they are computationally more expensive), as we approach the freezing and melting transition points the bare and bias protocols, respectively, become inefficient as the required decorrelation time grows exponentially with φ. Similar behavior is exhibited by the adaptive-bias scheme, albeit with a prolonged ability in reasonable long-range equilibration for volume fractions up to $\varphi \approx 0.56$. In contrast to all available implementations the proposed suite that bears CCAMs shows an exceptional efficiency for the whole density range even in the close vicinity of the MRJ state. By comparing the relaxation times for the $N_{av} = 12$ and 24 systems, it is immediately apparent that the performance of the adaptive-bias CCAM scheme remains unaffected by any increment in chain length, a feature in sharp contrast to every available technique (MC or MD) for the simulation of dense random packings of hard-sphere chains, yet reminiscent of the scaling behavior exhibited by the EB[50,61,73] and DB[49,51,62,66,74] moves in equilibrating entangled polymer melts. Additionally, packing density appears to have an almost negligible effect on the performance of the adaptive-bias, CCAM scheme as clearly shown in Figure 7. This unique (even for the established standards of the atomistic CCAMs) feature of the proposed MC protocol can be utterly attributed to the fact that both sEB and sIEB moves do not involve any kind of sphere displacement (even a minimal one), thus their acceptance rates are not affected by the densely packed environment around the chain-connectivity alteration.

Similar conclusions can be drawn by inspecting the diffusive behavior of the chain center-of-mass, shown in Figure 8, from

Table 5. Fitting a and b Parameters for the Scaling Relationship $\langle R^2\rangle = aN^b$, Where $\langle R^2\rangle$ Is the Mean Square End-to-End Distance and N Is the Chain Length

	$\varphi =$ 0.10	$\varphi =$ 0.20	$\varphi =$ 0.30	$\varphi =$ 0.40	$\varphi =$ 0.45	$\varphi =$ 0.50	$\varphi =$ 0.52	$\varphi =$ 0.54	$\varphi =$ 0.56	$\varphi =$ 0.58	$\varphi =$ 0.60	$\varphi =$ 0.61	$\varphi =$ 0.62	$\varphi =$ 0.63
a, $N_{av} = 12$	2.39	2.28	2.28	2.20	2.15	2.13	2.04	2.06	2.01	1.92	1.94	1.94	1.92	1.92
a, $N_{av} = 24$	3.48	3.19	3.13	2.88	2.73	2.68	2.47	2.45	2.35	2.36	2.35	2.38	2.37	2.38
b, $N_{av} = 12$	1.31	1.29	1.26	1.24	1.23	1.20	1.20	1.19	1.19	1.18	1.18	1.18	1.19	1.19
b, $N_{av} = 24$	1.18	1.17	1.14	1.14	1.14	1.11	1.13	1.12	1.12	1.11	1.11	1.10	1.10	1.11

MC simulations on $N_{av} = 12$ and 24 at $\varphi = 0.63$. The adaptive-bias scheme is utterly inefficient in displacing the chains since after hundreds of billions of MC steps chain centers have moved distances that are roughly comparable to the sphere diameter, σ. However, the MC mix that incorporates CCAMs, is so robust that the unphysical (due to chain-connectivity alternation) displacement of chains exceeds by orders of magnitude their dimensions (as quantified by the end-to-end distance) and the length of the simulation cell.

V.3. Bonded Geometry. As reported in the simulation findings of ref 60 as we approach the MRJ state for random chain assemblies bonded geometry (as quantified by the bond and torsion angle distribution) is heavily affected by packing density and the gradual adaptation of characteristic bending and torsional angles is preferred over the freely jointed pattern. Figure 9 exhibits the (supplement) bending angle distribution from simulations using the adaptive-bias and adaptive-bias CCAM schemes at $\varphi = 0.63$. Chain length appears to have an unnoticeable effect on bending geometry since the CCAM-generated distributions for the $N_{av} = 12$ and 24 systems are practically indistinguishable.[83] The adaptive-bias scheme provides a distribution of bending angles that follows that of the CCAM, albeit with a much pronounced statistical noise. This finding can be considered as a first (and clear) indication that the inclusion of CCAMs has an impact not only on long-range equilibration but also on the relaxation of local packing. The statement above is further documented by the corresponding simulation results for the torsion angle distribution shown in Figure 10. Sampling quality of the adaptive-bias scheme is very poor with respect to the torsion angles, whereas the CCAM-based mix samples correctly the dihedral angles characterizing the 1−4 packing along the chain for both simulated systems ($N_{av} = 12$ and 24). Primarily the results of Figure 10 about torsion angle distribution, and to a smaller extend the ones of Figure 9 about bending angle distribution, clearly suggest that the addition of CCAMs has a profound effect in the robust sampling of the local chain environment. The synergetic effect exhibited here adopts a twin role: localized moves (executed in the adaptive-bias scheme) act as "lubricants" for the long-range relaxation achieved by the CCAMs and in parallel CCAMs enhance the performance of the local moves by creating new trial patterns through continuous chain rearrangements that occur either within a single (sIEB) or a pair (sEB) of chains.

V.4. Chain Dimensions. Figure 11 presents the evolution of the running average value of the mean square end-to-end distance, $\langle R^2\rangle$, for the $N_{av} = 24$ system from MC simulations using the adaptive-bias, CCAM scheme at various packing densities. It is perfectly clear that, within modest CPU time and after a very small relaxation period that roughly corresponds to a dozen of billions MC steps, all simulated systems reach an equilibrium value of $\langle R^2\rangle$. Also shown in Figure 11 are corresponding results at $\varphi = 0.63$ but for the instantaneous value of $\langle R^2\rangle$. It is further evident that even at very high densities near the MRJ state ($\varphi = 0.63$) the proposed MC algorithm is capable of sampling quite robustly the configurational space of chain dimensions, as statistical fluctuations of $\langle R^2\rangle$ are quite large, and still the existence of a plateau value from the beginning of the trajectory is quite apparent.

Equilibrium results for the mean square end-to-end distance $\langle R^2\rangle$ were collected for all tested MC schemes and plotted as a function of packing density in Figure 12. Previous results in Figure 5−9 are confirmed also here since at dilute densities all schemes appear equally efficient in sampling the long-range dimensions of the athermal chains. In sharp contrast, as we reach higher volume fractions ($\varphi > 0.50$) all MC schemes, except the adaptive-bias CCAM, are "stuck" and they provide poor to unreliable predictions regarding the scaling of chain dimensions with packing density. It is only the adaptive-bias CCAM scheme that succeeds to predict the progressive chain collapsing for dense random packings, an effect that is strongly correlated with the adaptation of increasingly favorable bond and torsion angles as shown in Figures 9 and 10. This chain shrinkage can primarily be attributed to the existence of a gradually increasing population of successive triplets of hard-spheres with bending angles approximately equal to 60°, forming almost perfect equilateral triangles (corresponding to the most compact configuration between intramolecular neighbors that lie two bonds apart).

Figure 13 presents the simulation data for the dependence of $\langle R^2\rangle$ on φ in (natural-)logarithmic coordinates ($\ln(\langle R^2\rangle)$ vs $\ln(\varphi)$) for both simulated chain lengths. We can easily recognize three characteristic regimes for the $\langle R^2\rangle \sim \varphi^{-\gamma}$ scaling behavior: First, in the range $0.20 \le \varphi \le 0.40$ chain shrinkage is characterized by exponents of $\gamma \approx 0.23$ and 0.26 for the $N = 12$ and 24 systems, respectively. These values are in almost perfect agreement with previous simulations findings[31,32] and follow very closely the scaling concept of $\langle R^2\rangle \sim \varphi^{-\gamma}$ in the semidilute regime where $\gamma \approx (2\nu - 1)/(3\nu - 1) \approx 0.23$(with $\nu \approx 0.588$).[84] According to our simulation data this scaling regime of mild chain size reduction is followed by a much steeper chain collapse which occurs in the density range of $0.50 \le \varphi \le 0.60$ and is characterized by scaling exponents of $\gamma \approx 0.79$ and 0.90 for the $N_{av} = 12$ and 24 systems, respectively. Finally, in the close neighborhood of the MRJ state ($\varphi > 0.60$) chain dimensions appear to be virtually unaffected by any increment in volume fraction.

The execution of MC simulations on polydisperse samples of athermal chains, like the ones presented here, allows for the estimation of the scaling behavior of chain dimensions not only with respect to volume fraction φ (for a given N_{av}) but also to molecular length N (for a given φ). Figure 14 presents the dependence of $\langle R^2\rangle$ on N at various packing densities for (a) the $N_{av} = 12$ and (b) the $N_{av} = 24$ systems where each set of simulation data, for a given φ, is collected from a single NVT MC trajectory. We should note that for the common range of molecular lengths ($12 \le N \le 18$), for a given density, simulation data from both $N_{av} = 12$ and 24 coincide within the statistical error. For example at $\varphi = 0.63$, it is found that $\langle R^2\rangle_{N=12} = 38.4$ and 37.8 (where $\langle\rangle$ denote averaging over all recorded frames and all chains with length $N = 12$) from simulations on $N_{av} = 12$ and 24, respectively; also at the same volume fraction $\langle R^2\rangle_{N=18}$ was estimated at 61.8 and 60.6 for $N_{av} = 12$ and 24, respectively. In both cases the relative error is less than 2%,

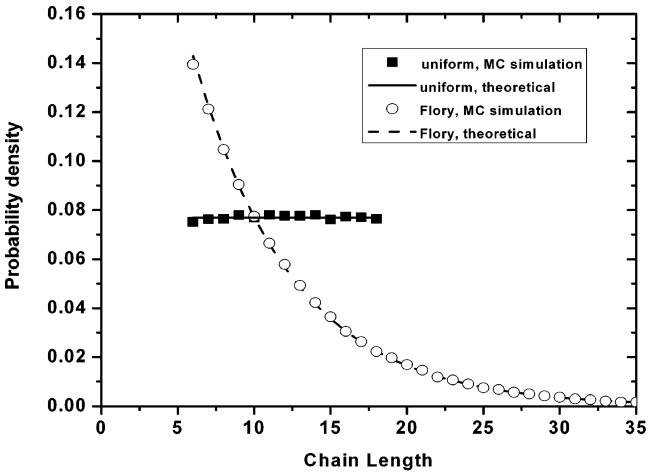

Figure 17. Chain length distributions as obtained from MC simulations on freely jointed hard-sphere chains with number-averaged degree of polymerization $N_{av} = 12$ at $\varphi = 0.10$ employing proper chemical potentials for (i) uniform ($\Delta = 0.5$) and (ii) most probable ($k_{min} = 6$) distributions. Also shown are corresponding data from theoretically predicted chain length distributions (see Appendix).

lying within the statistical uncertainty of the generated sample. In all sets of simulation data in Figure 14 the scaling of $\langle R^2 \rangle$ with N is almost linear as shown by the best linear fits for the $\varphi = 0.63$ collection of data points. A more accurate fit using the general expression $\langle R^2 \rangle = aN^b$ suggests that the calculated b exponents are higher than unity, suggesting a departure from the Gaussian coil concept, a trend that can be attributed to the small chain lengths studied here.[85] Fitted a and b parameters for the whole range of packing densities are summarized in Table 5. As expected both parameters get reduced with increasing packing density suggesting that the dense random structures behave closer to the ideal Gaussian chain concept.

V.5. Local Packing/Local Order. Results about the total radial distribution function, $g(r)$ and the chain form factor in Fourier space for high volume fractions are reported in ref 60, where a comparison is also presented with the corresponding results from simulations on hard-sphere monatomic analogs. In the present paper we present results about the intermolecular radial pair distribution function $g_{inter}(r)$ and the intrachain pair density function $w(r)$ in Figure 15 and Figure 16, respectively, for $N_{av} = 12$ and 24 at $\varphi = 0.20$ and 0.40. Regarding local packing our findings, in agreement with past simulations of Yethiraj and Dickman,[32] suggest that at low densities the probability of finding an intermolecular neighbor within the first coordination cell is reduced since any given sphere is surrounded by the tangent neighbors and other spheres that belong to the same chain. As density increases intermolecular pairs are brought closer together as indicated by the significant increment of the intensity of $g_{inter}(r)$ with increasing density for small radial distances. Characteristic sphere arrangements of intra- and intermolecular origins (as shown in both $g_{inter}(r)$ and $w(r)$) at $r = 1.0$ and $r \simeq 2.0$, are attributed the former to the nearest-neighbor distance and the latter to the existence of three-membered collineations as noted by Bernal.[16] In addition the sharp decline of the $w(r)$ curve at distances slightly higher than $r = 2.0$ suggest that the characteristic distance is a maximum indicative of a collineation.[16]

Local ordering for dense random assemblies is also analyzed in terms of crystalline symmetry norms, and it is found that as density increases a small, but progressively increasing, fraction of hard spheres possess highly ordered first coordination shell.[60]

VI. Conclusions/Future Plans

We have presented a MC scheme for the efficient generation and successive relaxation of dense random assemblies of freely jointed chains of hard spheres. The new protocol combines local MC moves, executed in an adaptive-bias pattern, and new advanced chain-connectivity altering moves that can function even in the close vicinity of the maximally random jammed (MRJ) state without being hindered by hard-sphere overlaps. The proposed combination vastly exceeds any available MC scheme in equilibrating both the short (as quantified by the distribution of bond and torsion angles) and long (as quantified by the end-to-end distance) chain characteristics.

The new MC scheme appears to scale as N^0 for the random generation of the amorphous cell (as long as systems with different N possess the same number of sites) and as $N^0\varphi^0$ for the equilibration of the long-range characteristics. It is applicable to any kind of force field that allows the close proximity (tangency) of intermolecular sites. Simulation findings, obtained with the new MC scheme, can be used to validate predictions of developed equations of state (EoS) for random chain packings close to the MRJ state.

Current efforts focus on the simulation of athermal systems characterized by much longer chain lengths to study the effect of packing density on a number of relevant statistics like entanglements (in the spirit of refs 86 and 87), local ordering, static scaling laws and the MRJ state. Extensions of the present MC suite to handle systems of variable molecular architecture (chain branching, absence of free ends, etc.) and to treat interactions at interfaces are in progress.

Appendix. Controlling Chain Length Distribution

In the present work we adopt the Pant−Theodorou[50] implementation to control molecular length distribution in polydisperse MC simulations. According to their approach while successful chain-connectivity altering moves (in our case the sEB and intermolecular reptation moves) change the molecular lengths of the participating chains, the chain length distribution (sampled over all existing chains N_{ch} of all recorded MC configurations) can be controlled by a proper selection of a spectrum of chemical potentials μ^*. If we define as N_k the number of chains that possess k hard spheres then we have for an m-component system[50]

$$n = \sum_{k=1}^{m} kN_k,\ N_{ch} = \sum_{k=1}^{m} N_k \qquad \text{(A.1)}$$

For systems where the values of N_{ch} and n are large one can relate N_k with μ^*_k through[50]

$$N_k = cy^k e^{\beta\mu_k^*} \qquad \text{(A.2)}$$

where index k runs over all m components except two (arbitrarily selected) i and j which are taken as reference species and for which it stands[50]

$$N_i = cy^i, \quad N_j = cy^j \qquad \text{(A.3)}$$

The c and y parameters are extracted by solving the system of eqs A.1−A.3.

In the following we present the chemical potentials and the corresponding molecular lengths, as defined by Pant and Theodorou, for the uniform and Flory (most probable) distributions for systems of freely jointed hard-sphere chains.

For the uniform distribution of chain lengths, the chemical potential are specified as[50]

$$\mu^*_k = -\infty, \quad k < N_{av}(1-\Delta) \text{ or } k > N_{av}(1+\Delta)$$
$$\mu^*_k = 0, \quad N_{av}(1-\Delta) \le k,i,j \le N_{av}(1+\Delta) \text{ and } k \neq i \neq j \tag{A.4}$$

which results in the following distribution of chain lengths

$$\frac{N_k}{N_{ch}} = 0, \quad k < N_{av}(1-\Delta) \text{ or } k > N_{av}(1+\Delta)$$
$$\frac{N_k}{N_{ch}} = \frac{1}{2\Delta N_{av}+1}, \quad N_{av}(1-\Delta) \le k \le N_{av}(1+\Delta) \tag{A.5}$$

Similarly, for the Flory distribution of chain lengths (with a lower threshold for chain lengths set at k_{min}) the chemical potentials are tuned as[50]

$$\mu^*_k = -\infty, \quad k < k_{min}$$
$$\mu^*_k = 0, \quad k,i,j \ge k_{min} \text{ and } k \neq i \neq j \tag{A.6}$$

corresponding to the following truncated exponential distribution of lengths

$$\frac{N_k}{N} = 0, \quad k < k_{min}$$
$$\frac{N_k}{N} = \frac{1}{N_{av}-k_{min}+1}\left(\frac{N_{av}-k_{min}}{N_{av}-k_{min}+1}\right)^{k-k_{min}}, \quad k \ge k_{min} \tag{A.7}$$

Figure 17 presents the uniform ($\Delta = 0.5$) and most-probable ($k_{min} = 6$) chain length distributions as obtained from MC simulations on polydisperse freely jointed hard-sphere chains with $N_{av} = 12$ at $\varphi = 0.10$ and the corresponding theoretical predictions based on eqs A.5 and A.7. It can be seen that there is an excellent agreement between expected and simulation-based resulted distributions of chain lengths. More details and an in-depth analysis of the correlation between chemical potential and chain length distribution can be found in the original paper by Pant and Theodorou.[50]

Acknowledgment. We are deeply grateful to financial support of the present project by the EC through contracts G5RD-CT-2002-00720 (PMILS) and NMP3-CT-2005-016375 (NSF-EC collaboration project MNIBS), and by CICYT through Contract MAT2005-25569-E. Generous allocation of computational time on the "Magerit" supercomputer of CeSViMa (UPM, Spain) is greatly appreciated.

References and Notes

(1) Cargill, G. S. *J. Appl. Phys.* **1970**, *41*, 12.
(2) Cargill, G. S. *J. Appl. Phys.* **1970**, *41*, 2248.
(3) Jullien, R.; Jund, P.; Caprion, D.; Quitmann, D. *Phys. Rev. E* **1996**, *54*, 6035.
(4) Ashcroft, N. W.; Lekner, J. *Phys. Rev.* **1966**, *145*, 83.
(5) Hales, T. C. *Ann. Math.* **2005**, *162*, 1065.
(6) Hales, T. C. *Discrete Comput. Geom.* **2006**, *36*, 5.
(7) Conway, J. H.; Sloane, N. J. A. *Sphere Packings, Lattices and Groups*; Springer-Verlag: New York, 1998.
(8) Bernal, J. D. *Nature (London)* **1959**, *183*, 141.
(9) Bernal, J. D. *Nature (London)* **1960**, *185*, 68.
(10) Bernal, J. D.; Mason, J. *Nature (London)* **1960**, *188*, 910.
(11) Scott, G. D.; Knight, K. R.; Bernal, J. D.; Mason, J. *Nature (London)* **1962**, *194*, 956.
(12) Bernal, J. D.; Finney, J. L. *Discuss. Faraday Soc.* **1967**, *43*, 62.
(13) Scott, G. D. *Nature (London)* **1960**, *188*, 908.
(14) Hoover, W. G.; Ree, F. H. *J. Chem. Phys.* **1968**, *49*, 3609.
(15) Scott, G. D.; Kilgour, D. M. *Br. J. Appl. Phys.* (*J. Phys. D*) **1969**, *2*, 863.
(16) Finney, J. L. *Proc. R. Soc. London A* **1970**, *319*, 479.
(17) Berryman, J. G. *Phys. Rev. A* **1983**, *27*, 1053.
(18) Jodrey, W. S.; Tory, E. M. *Powder Technol.* **1981**, *30*, 111.
(19) Jodrey, W. S.; Tory, E. M. *Phys. Rev. A* **1985**, *32*, 2347.
(20) Clarke, A. S.; Wiley, J. D. *Phys. Rev. B* **1987**, *35*, 7350.
(21) Richard, P.; Oger, L.; Troadec, J.-P.; Gervois, A. *Phys. Rev. E* **1999**, *60*, 4551.
(22) Torquato, S.; Truskett, T. M.; Debenedetti, P. G. *Phys. Rev. Lett.* **2000**, *84*, 2064.
(23) Donev, A.; Stillinger, F. H.; Torquato, S. *Phys. Rev. Lett.* **2005**, *95*, 090604.
(24) Donev, A.; Torquato, S.; Stillinger, F. H. *Phys. Rev. E* **2005**, *71*, 011105.
(25) Donev, A.; Torquato, S.; Stillinger, F. H. *J. Comput. Phys.* **2005**, *202*, 737.
(26) Donev, A.; Torquato, S.; Stillinger, F. H. *J. Comput. Phys.* **2005**, *202*, 765.
(27) Lubachevsky, B. D.; Stillinger, F. H. *J. Stat. Phys.* **1990**, *60*, 561.
(28) Dickman, R. R.; Hall, C. K. *J. Chem. Phys.* **1988**, *89*, 3168.
(29) Muthujumar, M.; Baumgärtner, A. *Macromolecules* **1989**, *22*, 1941.
(30) Denlinger, M. A.; Hall, C. K. *Mol. Phys.* **1990**, *71*, 541.
(31) Yethiraj, A.; Hall, C. K. *J. Chem. Phys.* **1992**, *96*, 797.
(32) Yethiraj, A.; Dickman, R. *J. Chem. Phys.* **1992**, *97*, 4468.
(33) Chang, J.; Sandler, S. I. *Chem. Eng. Sci.* **1994**, *49*, 2777.
(34) Li, X. J.; Chiew, Y. C. *J. Chem. Phys.* **1994**, *101*, 2522.
(35) O'Lenick, R.; Li, X. J.; Chiew, Y. C. *Mol. Phys.* **1995**, *86*, 1123.
(36) Escobedo, F. A.; de Pablo, J. J. *Macromol. Theory Simul.* **1995**, *4*, 691.
(37) Escobedo, F. A.; de Pablo, J. J. *J. Chem. Phys.* **1995**, *102*, 2636.
(38) Malanoski, A. P.; Monson, P. A. *J. Chem. Phys.* **1997**, *107*, 6899.
(39) Haslam, A. J.; Jackson, G.; McLeish, T. C. B. *J. Chem. Phys.* **1999**, *111*, 416.
(40) Haslam, A. J.; Jackson, G.; McLeish, T. C. B. *Macromolecules* **1999**, *32*, 7289.
(41) Lin, C.-T.; Stell, G.; Kalyunhnyi, Y. V. *J. Chem. Phys.* **2000**, *112*, 3071.
(42) Vega, C.; McBride, C.; MacDowell, L. G. *J. Chem. Phys.* **2001**, *115*, 4203.
(43) Cochran, T. W.; Chiew, Y. C. *J. Chem. Phys.* **2006**, *124*, 074901.
(44) Chang, R.; Yethiraj, A. *Phys. Rev. Lett.* **2006**, *96*, 107802.
(45) Kröger, M. *Comput. Phys. Commun.* **1999**, *118*, 278.
(46) Kröger, M.; Müller, M.; Nievergelt, J. *Comput. Model. Eng. Sci.* **2003**, *4*, 559.
(47) Tobochnik, J.; Chapin, P. M. *J. Chem. Phys.* **1988**, *88*, 5824.
(48) Allen, M. P.; Tildesley, D. J. *Computer Simulation of Liquids*; Clarendon: Oxford, U.K., 1987.
(49) Karayiannis, N. C.; Mavrantzas, V. G. *Macromolecules* **2005**, *38*, 8583.
(50) Pant, P. V. K.; Theodorou, D. N. *Macromolecules* **1995**, *28*, 7224.
(51) Karayiannis, N. C.; Mavrantzas, V. G.; Theodorou, D. N. *Phys. Rev. Lett.* **2002**, *88*, 105503.
(52) Uhlherr, A.; Mavrantzas, V. G.; Doxastakis, M.; Theodorou, D. N. *Macromolecules* **2001**, *34*, 8554.
(53) Banaszak, B. J.; de Pablo, J. J. *J. Chem. Phys.* **2003**, *119*, 2456.
(54) Auhl, R.; Everaers, R.; Grest, G. S.; Kremer, K.; Plimpton, S. J. *J. Chem. Phys.* **2003**, *119*, 12718.
(55) Bishop, M.; Ceperley, D.; Frisch, H. L.; Kalos, M. H. *J. Chem. Phys.* **1980**, *72*, 3228.
(56) Vacatello, M.; Avitabile, G.; Corradini, P.; Tuzi, A. *J. Chem. Phys.* **1980**, *73*, 548.
(57) Siepmann, J. I.; Frenkel, D. *Mol. Phys.* **1992**, *75*, 59.
(58) de Pablo, J. J.; Laso, M.; Suter, U. W. *J. Chem. Phys.* **1992**, *96*, 2395.
(59) Dodd, L. R.; Boone, T. D.; Theodorou, D. N. *Mol. Phys.* **1993**, *78*, 961.
(60) Karayiannis, N. C.; Laso, M. *Phys. Rev. Lett.* **2008**, in press.
(61) Mavrantzas, V. G.; Boone, T. D.; Zervopoulou, E.; Theodorou, D. N. *Macromolecules* **1999**, *32*, 5072.
(62) Karayiannis, N. C.; Giannousaki, A. E.; Mavrantzas, V. G.; Theodorou, D. N. *J. Chem. Phys.* **2002**, *117*, 5465.
(63) Any relaxed chain configuration can be decomposed into a (non-overlapping) set of single hard-spheres ($N_{av} = 1$) corresponding to the same packing density for successive simulations of monoatomic hard-sphere analogs.
(64) Mavrantzas, V. G.; Theodorou, D. N. *Macromolecules* **1999**, *31*, 6310.
(65) Wall, F. T.; Mandel, F. *J. Chem. Phys.* **1975**, *63*, 4592.
(66) Karayiannis, N. C.; Giannousaki, A. E.; Mavrantzas, V. G. *J. Chem. Phys.* **2003**, *118*, 2451.
(67) Frenkel, D.; Mooij, G. C. A. M.; Smit, B. *J. Phys.: Condes. Matter* **1991**, *3*, 3053.

(68) Siepmann, J. I.; McDonald, I. R.; Frenkel, D. *J. Phys.: Condens. Matter* **1992**, *4*, 679.
(69) de Pablo, J. J.; Laso, M.; Suter, U. W. *J. Chem. Phys.* **1992**, *96*, 6157.
(70) Laso, M.; de Pablo, J. J.; Suter, U. W. *J. Chem. Phys.* **1992**, *97*, 2817.
(71) Leontidis, E.; de Pablo, J. J.; Laso, M.; Suter, U. W. *Adv. Polym. Sci.* **1994**, *116*, 283.
(72) Peristeras, L. D.; Economou, I. G.; Theodorou, D. N. *Macromolecules* **2005**, *38*, 386.
(73) Theodorou, D. N. In *Molecular Simulations for the Next Decade*; Nielaba, P., Mareschal, M., Ciccotti, G., Eds.; Springer-Verlag: Berlin, 2002.
(74) Karayiannis, N. C.; Mavrantzas, V. G. In *Multiscale Modelling of Polymer Properties* (*Computer-Aided Chemical Engineering 22*); Perpète, E., Laso, M., Eds.; Elsevier: Amsterdam, 2006.
(75) Doxastakis, M.; Mavrantzas, V. G.; Theodorou, D. N. *J. Chem. Phys.* **2001**, *115*, 11339.
(76) The notation "CCB" is obviously misleading in the case of CCB when $n_{dis} = 1$ as there is no biased selection involved in the move. A more accurate description would be "regrowth of end-segments", but in order to be consistent with previous CCB-based modeling studies we have maintained the "CCB" title to even denote the bare execution.
(77) Laso, M.; Karayiannis, N. C.; Müller, M. *J. Chem. Phys.* **2006**, *125*, 164108.
(78) Theodorou, D. N. *J. Chem. Phys.* **2006**, *124*, 034109.
(79) Bunker, A.; Dünweg, B. *Phys. Rev. E* **2000**, *63*, 016701.
(80) Jagannathan, K.; Sung, B. J.; Yethiraj, A. *Phys. Rev. Lett.* **2006**, *97*, 145503.
(81) One could claim that for very dilute athermal systems direct application of MC schemes based solely on the CCB algorithm is adequate even for long chains.
(82) The conclusion presented here is valid only for small chain lengths at dilute densities. As will be shown in a future publication the long-range equilibration of much longer chains ($N_{av} = 1000$) is greatly benefited by the application of the adaptive-bias, CCAM scheme built around the sIEB algorithm.
(83) The argument is valid for the whole density range simulated in the course of the present work.
(84) deGennes, P.-G. *Scaling Concepts in Polymer Physics*; Cornell University: Ithaca, NY, 1979.
(85) Preliminary simulations with much longer chain lengths ($N_{av} = 1000$) suggest that the scaling exponents are in excellent agreement with the Gaussian coil predictions.
(86) Foteinopoulou, K.; Karayiannis, N. C.; Mavrantzas, V. G.; Kröger, M. *Macromolecules* **2006**, *39*, 4207.
(87) Tzoumanekas, C.; Theodorou, D. N. *Macromolecules* **2006**, *39*, 4592.

MA702264U